Published in final edited form as:
Nano Lett. 2009 October ; 9(10): 3612–3618. doi:10.1021/nl9018275.

Dynamic Imaging of Molecular Assemblies in Live Cells Based on Nanoparticle Plasmon Resonance Coupling

Jesse Aaron[1], **Kort Travis**[2], **Nathan Harrison**[2], and **Konstantin Sokolov**[1,3,*]

[1]Dept. Biomedical Engineering, University of Texas at Austin, Austin, TX 78712

[2]Dept. Physics, University of Texas at Austin, Austin, TX 78712

[3]Dept. Imaging Physics, UT MD Anderson Cancer Center, Houston, TX 77030

Abstract

We used molecular-specific gold nanoparticles to monitor epidermal growth factor receptors (EGFR) in live A431 cells over time. Dark-field hyperspectral imaging, electron microscopy, and electrodynamic modeling were used to correlate optical properties of EGFR-bound plasmonic nanoparticles with receptor regulation state. We showed that receptor trafficking resulted in a progressive red-shift of greater than 100nm in the nanoparticle plasmon resonance wavelength over a time period of 60 minutes. Furthermore, we demonstrated that changes in peak scattering wavelengths of gold nanoparticles from 546±15 nm to 574±20 nm and, to 597±44 nm are associated with EGFR trafficking from the cell membrane, to early endosomes and to late endosomes/multi-vesicular bodies, respectively. Finally, we used the changes in scattering spectra of EGFR-bound nanoparticles and a straightforward statistical analysis of RGB-channel color images of labeled cells to create near real-time maps of EGFR regulatory states in living cells.

Keywords

plasmonic nanoparticles; molecular imaging; functional imaging; growth factor receptors; molecular trafficking

Detecting and monitoring the vast number of bio-molecular interactions in the cell is a central effort in biology, as these interactions largely govern the behavior of nearly all cell types. Imaging methods are an indispensable approach for measuring the spatio-temporal characteristics of protein assemblies in intact cells. In this work, we expand the application of nanoparticle plasmon resonance coupling (NPRC) and demonstrate a novel, generalized method for imaging and characterizing molecular assemblies at the nanometer length-scale in living cells.

Over the past decades, fluorescence resonance energy transfer (FRET) has allowed many investigators to elucidate important functional associations between pairs of proteins at sub-microscopic resolution, all without destroying the cell[1]. More recently, techniques such as image correlation microscopy (ICM) and its variants have been widely used to characterize larger protein assemblies and clusters, including EGFR, *in-situ*2, 3. Although all of these techniques are eminently useful, FRET is typically limited to detecting two very closely separated (< 5nm) molecules of different types1, 4. While the various ICM methods can be

*CORRESPONDING AUTHOR: Tel: 512-471-7440; kostia@mail.utexas.edu.

SUPPORTING INFORMATION AVAILABLE. Detailed description of Methods. This material is available free of charge via the Internet at http://pubs.acs.org.

used to evaluate associations and clustering between many molecules on the submicron scale, this additional information is an ensemble average and it does not directly reveal the distribution of cluster sizes or any additional information related to nanometer-scale organization of biomolecules forming the clusters[2, 3]. Furthermore, ICM methods are in general highly sensitive to background interference, and the resolution of the imaging system is often not fully utilized. In addition, both FRET and ICM can be critically limited by photobleaching. These limitations are avoided in electron microscopy (EM), and in particular, the immuno-gold method to image assemblies of biomolecules at the nanometer length scale[5]. However, this comes at the expense of the lack of real-time, live-cell capability and of additional tedious sample preparation. For all of these reasons, new physical methods are required that extend and or complement currently available capabilities for quantitative monitoring of molecular clusters with high spatial and temporal resolution in living cells.

Recently, plasmonic-resonant nanoparticles have been explored as molecular-specific probes for highly sensitive detection[6–16] and for photothermal damage of cells[17–20]. When two or more plasmonic nanoparticles are in close proximity they exhibit the effect of nanoparticle plasmon resonance coupling (NPRC) which manifests as a spectral shift in the optical cross sections of the metal nanoparticle assemblies, when compared to those observed from the isolated nanoparticles[21, 22]. This spectral shift is strongly dependent on the inter-particle distance[23], and the sensitivity can be conveniently adjusted by modifying the particle size. NPRC is significant for particle center-to-center distances of less than about three times the particle radius, thus providing a useful range of detectable interaction distances out to tens of nanometers. Because of this behavior, NPRC has recently been demonstrated as an attractive analog to FRET, as evidenced by its use in the detection of DNA-DNA[24–26], DNA-protein[27], and protein-protein binary interactions[28]. These investigations showed that NPRC is not limited by photo-bleaching and that it can extend the range of detectable distances by more than an order of magnitude in comparison to FRET.

We have shown previously that NPRC provides a powerful cancer diagnostic method by facilitating the detection of growth factor receptor clustering in cancerous tissue[6, 29]. In the present work, we expand the applicability of NPRC to the study of molecular clustering and regulation mechanisms in living cells. We have developed a novel computational framework to gain nanometer-scale information from NPRC spectra, and in addition, a practical image-analysis method to infer growth factor receptor regulation state.

We monitor the trafficking mechanisms of the epidermal growth factor receptor (EGFR) – a receptor tyrosine kinase (RTK) that controls some of the most fundamental cellular processes including DNA replication and cell division[30]. EGFR is also an important cancer biomarker with regulatory pathways that have profound implications for the development of new cancer therapeutics[31, 32]. The EGFR internalization process is a key regulatory pathway that determines cell behavior. It is well-known that membrane-bound EGFR elicits growth-promoting signals upon ligand binding. However, it has recently been shown that signaling can continue even after internalization of EGFR in early endosomes and that the signaling activity finally ceases after entry into lysosomes[31]. Further, processes involving EGFR recycling and nuclear translocation add to the complexity of EGFR's role[30, 33]. Thus, it is vital that an effective EGFR imaging strategy not only involves detection of the protein, but also includes the nanometer-scale details of its organization, aggregation, and sequestration within cellular compartments. In this study, we demonstrate that NPRC is a convenient method that facilitates the retrieval of this information using dark-field color imaging of live cells labeled with EGFR-specific gold nanoparticles.

Synthesis of molecular specific gold nanoparticles

Near-spherical gold nanoparticles (with average diameter of 25nm) were synthesized using the method described by Frens, whereby chloroauric acid ($HAuCl_4$) is chemically reduced using sodium citrate[34]. By altering the Au^{3+} to citrate ratio, the size of the resulting nanoparticles can be controlled. For the size of particles used in the present work, this protocol produces gold colloid with a particle concentration of approximately 6×10^{11} particles per milliliter.

To conjugate monoclonal antibodies to the surfaces of the gold nanoparticles, a hetero-bifunctional linker was utilized, as described in[35]. Briefly, anti-EGFR monoclonal antibodies (clone 29.1.1 Sigma) were purified from acites fluid using a 100 kDa MWCO centrifugal filter, and resuspended in 40mM HEPES solution (pH 7.5) at a concentration of 1 mg/mL. Sodium periodate (NaIO4) was added to the antibody solution at a final concentration of 10 mM for 30 minutes under mild agitation, and protected from the light. Sodium periodate oxidizes the hydroxyl moieties located on the glycosylated Fc region of antibodies to aldehyde groups. Then, the solution was diluted 50-fold using 1× PBS, and 200 μM of a heterobifunctional linker was added (Sensopath Technologies, Inc.). The linker consists of a PEG chain containing two sulfhydril groups on one end, and a hydrazide moiety on the other. The newly formed aldehydes on the antibodies condense with the hydrazide group on the linker, leaving the thiols available for binding to the gold surface. Excess unreacted linker was removed via centrifugal filtration as described above, and the antibody-linker solution was stored at 1mg/mL in 1× PBS for up to 4 weeks. Prior to cell labeling, the antibody-linker solution was first diluted 100-fold in 40mM HEPES solution, to which an equal volume of 25nm gold nanoparticles was added. The two components were allowed to mix under mild agitation for 20 minutes, followed by addition of 5 kDa monofunctional thiolated polyethylene glycol (mPEG-SH, Nektar) to 10^{-6} M final concentration. Five minutes after addition of mPEG-thiol antibody-nanoparticle conjugates were spun down at 3400 × g for 30 minutes, the supernatant removed, and the conjugates re-suspended in phenolphthalein-free DMEM cell culture media (Gibco) containing 10% FBS.

Gold particles of 25 nm diameter were used because they provide high contrast in detection of EGFR over-expressing A431 cells29. The particles were conjugated with antibodies that do not block receptor activation by EGF[36]. We have demonstrated in previous studies that nanoparticles conjugated with either monofunctional thiolated polyethylene glycol (mPEG-SH) or a non-specific antibody do not interact with EGFR expressing cells. Further, specificity of EGFR binding by the gold conjugates was shown by displacement and competition assays in the presence of free anti-EGFR antibodies[29].

Dynamic imaging of live cells

A431 keratinocytes were cultured on 22 mm square glass coverslips using DMEM/F-12 (50/50) growth medium, supplemented with 5% FBS (Gibco), in a 37°C and 5% CO2 environment. For live imaging experiments, A431 cells were seeded onto optical imaging flow chambers (ibidi μslide chambers, Integrated BioDiagnostics), and allowed to adhere overnight. Then, the chambers were separated into two samples: chambers where cells were exposed to 10 μM AG1478 (Calbiochem), a EGFR phosphorylation inhibitor[37], and control chambers where cells were not exposed to the inhibitor. The samples were then kept for another 24 hours under serum-starvation conditions. Chambers were placed under the microscope and connected to a peristaltic pump supplying either DMEM (containing 10% FBS) media or gold nanoparticle conjugates in complete DMEM at low flow rates (typically < 1mL/min). Temperature control of solutions was accomplished through the use of an in-line resistive heater (Harvard Apparatus) to 37°C before being introduced into the chamber.

Samples were continuously exposed to conjugates at approximately 10^{12} particles/mL under low flow conditions for 45–60 minutes during time-lapse imaging. Cell samples were imaged

using a Leica DM6000 upright microscope, a 100W halogen light source and an oil-immersion darkfield condenser (Leica) with an N.A. of 1.2. A long-working distance (1.2mm), 63× objective (Leica) with 0.75 NA was used for collection of scattering signal and the images were recorded by a high-sensitivity 12-bit color-mosaic CCD camera (SPOT Pursuit XS, Diagnostic Instruments). To ensure cell viability over the duration of live imaging experiment, we carried out Calcein AM assay (Molecular Probes) after 2 hours of cell exposure to anti-EGFR nanoparticle conjugates. Results (figure available in online Supporting Information) showed that there are no statistically significant changes in cell viability between cells treated with gold nanoparticles and unlabeled controls.

Dynamic imaging of live cells labeled with anti-EGFR nanoparticles exhibited a progressive color change from green to yellow, and finally, to orange-red (Figure 1, B). The color changes are well-correlated in time with known trafficking dynamics of EGFR (Figure 1, A)[33, 38]. Initially, EGFR molecules dimerize and aggregate in the plasma membrane, followed by endocytosis into early endosomes. These early endosomes can then either recycle to the cell surface, or proceed through formation of late endosomes and MVBs within 20–60 minutes[33, 38]. The effect of continuous color changes was disrupted by a potent EGFR inhibitor, AG1478, which interferes with EGFR trans-phosphorylation and internalization (Figure 1, C)[37]. These data indicate that the observed color changes are associated with EGFR re-organization within the cell both as a result of ligand binding, and also due to intracellular trafficking in vesicles. In images taken from untreated samples, the relative intensity of the red channel increases from 27% to nearly 34% (Figure 1, B) whereas for samples treated with AG1478 inhibitor, this value increases only from 28% to 30% (Figure 1, C).

Cell labeling at different temperatures

In order to establish a relationship between the scattering behavior of EGFR-bound plasmonic nanoparticles and the dynamics of EGFR regulation in live cells we carried out labeling at 4° C, 25°C, and 37°C. Temperature control allows the activation and trafficking mechanisms of EGFR to be arrested at critical points: EGFR internalization is inhibited in cells at 4°C; internalization proceeds to formation of early endosomes at 25°C; and finally, complete EGFR regulation proceeds through the formation of multivesicular bodies (MVB) and late endosomes within an hour at 37°C[33, 38,39].

For the temperature-based experiments, cells were seeded onto coverslips at between 50,000–100,000 cells/mL and left to adhere overnight. Then, cells were washed in 1× PBS, and 1mL of gold nanoparticle bioconjugates in DMEM supplemented with 5% FBS was added. Coverslip-adherent cell samples containing nanoparticles were placed in 4°C, 25°C, and 37° C environments and allowed to interact for 60 minutes. Nanoparticles were then aspirated from the sample, followed by washing in 1× PBS, and fixation with freshly prepared 4% formaldehyde at 4°C for 15 minutes. Color images of cells labeled at the three temperature points showed a readily observable changes from green (4°C, Figure 2, a) to yellow (25°C, Figure 2, b) and, finally, to orange-red (37°C, Figure 2, c) color in the scattering signal. The corresponding transmission electron microscopy (TEM) images of labeled cells (Figure 2, d–f) showed the temperature-dependent changes in the nanometer-scale organization of EGFR that had been reported by others[39]. At 4°C, nanoparticles are located on the cell membrane in small clusters. Increasing the temperature to 25°C results in a more three-dimensional, volume-filling aggregate morphology which is consistent with endosomal uptake. At 37°C, progression of EGFR trafficking leads to appearance of an even more complicated aggregate structure corresponding to MVBs, which are destined for EGFR degradation.

We used hyperspectral imaging to quantify the nanoparticle scattering changes in relation to EGFR behavior (Figure 3, a–i). Hyperspectral images were acquired using the PARISS®

system (Lightform, Inc.). Scattering peaks in the range of 530–550 nm are present in images obtained at 4°C (Figure 3, d); at this temperature EGFR is predominantly located on the cytoplasmic membrane. Increased red-shifting of the peaks becomes apparent at 25°C with EGFR located predominantly in early endosomes (Figure 3, e), while a wide range of scattering peak positions is evident at 37°C (Figure 3, f). At 4°C and 25°C (Figure 3, g and h, respectively), labeled cells display peak wavelength distributions with mean and standard deviation values of 546±15 nm and 574±20 nm, respectively. Interestingly, at 37°C (Figure 3, i), there is a large degree of heterogeneity in peak scattering wavelengths (mean and standard deviation - 597±44 nm), this is consistent with the simultaneous presence of multiple regulation/trafficking stages of EGFR within the cell.

Electrodynamic Modeling of Light Scattering from Metal Nanoparticle Aggregates

In order to further explore the relationship between nanoparticle aggregate morphology and the associated optical cross sections, we implemented detailed electrodynamic simulations. The computational electrodynamics codes used for the nanoparticle aggregate simulations are part of a new T-matrix code-base implemented entirely in C++, which has been developed over the past several years[40]. A hybrid multi-threaded message-passing-interface (MPI) task model is used throughout, allowing optimal utilization of modern cluster-computing resources. The specific T-matrix formulation used, as extended to aggregates, is based primarily on the methods discussed in Mackowski, Mishchenko,[41–]43 and Stout44. The specifics of the permittivity functions used are described in Aaron et al45. In all cases, incident illumination is unpolarized, with wave-vector directed into the page as the rendered structures are shown (Figure 3, m–o). Gold spheres are 25 nm in diameter, surrounded by water, with mean interparticle center-to-center spacing of 2.4 times the particle radius. The particles are normally distributed in 3-D about ideal lattice-points with a fractional standard deviation of 0.07. For each of the aggregate morphologies, simulation structures were constructed using typical values for aggregate particle number, inter-particle spacing, and overall morphology as indicated from the TEM images.

The optical behavior of nanoparticle aggregates has a complicated, non-linear dependence on details of the aggregate morphology, in addition to a greatly enhanced optical cross section which varies in general quadratically as the number of particles in the aggregate29, [40]. The details of aggregate morphology may include receptor/nanoparticle number, spacing, and overall arrangement in space (such as 2D planar or a more 3D volume-filling configuration). In general, the effect of inter-particle coupling produces a red-shift and broadening of the resonance peak. Figure 3(j–l) shows scattering cross-sections from three typical structures (Figure 3, m–o) which were designed to approximate the aggregate morphology indicated in Figure 2(d–f). Note that the simulated spectra show the overall red-shifting and peak broadening, consistent with spectra shown in Figure 3(a×c).

For random aggregates, due to the high-order, non-linear dependence of the plasmonic resonance coupling on the inter-particle spacing, small statistical fluctuations in particle position about the mean have a significant effect on spectral shift[40]. In addition, three-dimensional more volume-filling aggregates, such as those seen in endosomes, experience significantly more spectral shift than two-dimensional aggregates. This is noteworthy because it indicates that NPRC can detect differences in

Monitoring of EGFR trafficking

Having established the relationship between the scattering properties of EGFR-bound nanoparticles and EGFR regulatory stages, we examined the degree to which RGB imaging

could be effectively employed to monitor EGFR trafficking. It appeared that the increase in the relative intensity of the red channel in color images of live cells (Figure 1, B) was a pronounced indicator of EGFR activation and endocytosis. Therefore, we used this parameter to correlate color changes in live cell images with EGFR regulatory stages. To accomplish this, the hyperspectral data presented in Figure 3 were grouped into three categories, corresponding to the associated EGFR regulatory states: (1) surface receptors, (2) early endosomes, and (3) late endosomes/MVBs. Pixel-data from at least five complete cells were analyzed in each group, representing at least 1000 spectra per group. The resulting spectra were used to obtain statistically distinct distributions for intensity-normalized red channel values characteristic for each EGFR state (Figure 4). Then, for each non-background pixel in the time-lapse images (shown in Figure 1), we determined the probability that its normalized red channel value falls within each of the distributions associated with EGFR states (Figure 4). These paired comparisons resulted in three p-values that were used as weighting factors in assigning a pseudo-color to each pixel in live cell images. This analysis resulted in images where color represents a statistical probability of a regulatory stage of EGFR (Figure 5).

In contrast to previous studies that employed fluorescent tags such as quantum dots[46] to monitor EGFR trafficking the use of plasmonic resonant nanoparticles provides additional information about proximity and nanometer-scale organization of biomolecules. It has been shown that the optical changes corresponding to inter-particle distance between nanoparticle pairs can be precisely quantified[23] and work is under way to develop a similarly quantified model for nanoparticle aggregates[40].

The application of NPRC described here can be extended to other RTKs and G-protein-coupled receptors that are involved in signal transduction[33]. Other molecular systems for investigation may include integrin clustering and immunological synapse formation. This method can potentially be applied to hetero-molecular interactions such as interactions between different RTKs if the interacting molecules are labeled with plasmonic nanoparticles that exhibit distinct optical properties. Theoretical simulations that are described here can be used to optimize the design of nanoparticles which would produce distinct optical changes in the case of homo- and hetero-interactions.

A primary strength of NPRC as a biosensing tool is associated with the complex optical behavior of plasmonic nanoparticle assemblies. The dramatic changes in optical properties associated with nanometer-scale changes in organization facilitate the development of statistical associations with the biological processes under observation. Further understanding of NPRC will be vital for its development as a quantitative biosensing tool. Issues such as particle shape heterogeneity, as well as the more nuanced effects of nanoparticle aggregate morphology on spectral characteristics (such as scattering peak width) are still under study, and promise to reveal a wealth of additional information. NPRC can be used as an independent method or it can potentially be integrated into already in-use biophysical methods such as FRET[1], 4, ICM2, 3, or EM[5] to provide additional complimentary information. TEM with immunogold labels has been used to study 3D organization of proteins with high spatial resolution in fixed samples. The method presented here allows extending this TEM imaging approach to live-cell dynamic optical imaging of molecular assemblies with unambiguous information about the proximity and nanometer-scale organization of biomolecules. While not strictly a super-resolution method, NPRC can provide sub-diffraction characterization capability over distances ranging from a few tens of nanometers which significantly exceed distances available through FRET. In addition, NPRC exhibits sensitivity to geometrical characteristics of protein clusters such as a planar 2D or a volume-filling 3D aggregation in live-cell imaging and it is capable of following cluster dynamics in real time. The sensitivity of NPRC to nanometer-scale geometry of individual clusters can potentially provide invaluable complementary information to ensemble population measurements such as cluster density and

the average number of receptors per cluster that are afforded by ICM methods. Further, gold nanoparticles themselves can make excellent probes for ICM, due to their brightness and photostability, which will facilitate the direct combination of these techniques. We anticipate that NPRC will continue to gain interest among biological and biomedical researchers as a method to produce unique insight into biomolecular interactions.

Supplementary Material

Refer to Web version on PubMed Central for supplementary material.

Acknowledgments

We gratefully acknowledge support from National Cancer Institute grant R01 CA103830 BRP.

References

1. Jares-Erijman EA, Jovin TM. Current Opinion in Chemical Biology 2006;10(5):409–416. [PubMed: 16949332]
2. Bates IR, Wiseman PW, Hanrahan JW. Biochemistry and Cell Biology 2006;84:825–831. [PubMed: 17215870]
3. Clayton AHA, Walker F, Orchard SG, Henderson C, Fuchs D, Rothacker J, Nice EC, Burgess AW. Journal of Biological Chemistry 2005;280(34):30392–30399. [PubMed: 15994331]
4. Vogel SS, Thaler C, Koushik SV. Science STKE 2006;2006(331):re2.
5. Horisberger M, Rosset J, Bauer H. Experientia 1975;31(10):1147–1149. [PubMed: 1107057]
6. Sokolov K, Follen M, Aaron J, Pavlova I, Malpica A, Lotan R, Richards-Kortum R. Cancer Research 2003;63(9):1999–2004. [PubMed: 12727808]
7. Sokolov K, Aaron J, Hsu B, Nida D, Gillenwater A, Follen M, MacAuley C, Adler-Storthz K, Korgel BA, Descour M, Pasqaulini R, Arap W, Lam W, Richards-Kortum R. Technology in Cancer Research and Treatment 2003;2(5):491–504. [PubMed: 14640761]
8. Loo C, Lin A, Hirsch L, Lee M-H, Barton J, Halas N, West J, Drezek R. Technology in Cancer Research & Treatment 2004;3(1):33–40. [PubMed: 14750891]
9. El-Sayed IH, Huang X, El-Sayed MA. Nano Letters 2005;5(5):829–834. [PubMed: 15884879]
10. Loo C, Lowery A, Halas N, West J, Drezek R. Nano Letters 2005;5(4):709–711. [PubMed: 15826113]
11. Skala MC, Crow MJ, Wax A, Izatt JA. Nano Letters 2008;8(10):3461–3467. [PubMed: 18767886]
12. Alivisatos P. Nature Biotechnology 2004;22(1):47–52.
13. Aslan K, Lakowicz JR, Geddes CD. Current Opinion in Chemical Biology 2005;9(5):538–544. [PubMed: 16129649]
14. Mallidi S, Larson T, Aaron J, Sokolov K, Emelianov S. Optics Express 2007;15(11):6583–6588. [PubMed: 19546967]
15. Yang X, Skrabalak SE, Li ZY, Xia Y, Wang LV. Nano Lett 2007;7(12):3798–3802. [PubMed: 18020475]
16. Curry A, Crow MJ, Wax A. Journal of Biomedical Optics 2008;13:014022. [PubMed: 18315380]
17. Huang X, El-Sayed IH, Qian W, El-Sayed MA. Journal of the American Chemical Society 2006;128 (6):2115–2120. [PubMed: 16464114]
18. Hirsch LR, Stafford RJ, Bankson JA, Sershen SR, Rivera B, Price RE, Hazle JD, Halas NJ, West JL. Proceedings of the National Academy of Sciences of the United States of America 2003;100(23): 13549–13554. [PubMed: 14597719]
19. Larson TA, Bankson J, Aaron J, Sokolov K. Nanotechnology 2007;18:325101.
20. Chen J, Wang D, Xi J, Au L, Siekkinen A, Warsen A, Li ZY, Zhang H, Xia Y, Li X. Nano Letters 2007;7(5):1318–1322. [PubMed: 17430005]
21. Kreibig, U.; Volmer, M. Optical Properties of Metal Clusters. Berlin, Germany: Springer; 1995.
22. Rechberger W, Hohenau A, Leitner A, Krenn JR, Lamprecht B, Aussenegg FR. Optics Communications 2003;220(1–3):137–141.

23. Jain PK, Huang W, El-Sayed MA. Nano Letters 2007;7(7):2080–2088.
24. Elghanian R, Storhoff JJ, Mucic RC, Letsinger RL, Mirkin CA. Science (Washington, D. C.) 1997;277 (5329):1078–1080.
25. Soennichsen C, Reinhard BM, Liphardt J, Alivisatos AP. Nature Biotechnology 2005;23(6):741–745.
26. Storhoff JJ, Lucas AD, Garimella V, Bao YP, Mueller UR. Nature Biotechnology 2004;22(7):883–887.
27. Reinhard, BrM; Sheikholeslami, S.; Mastroianni, A.; Alivisatos, AP.; Liphardt, J. Proceedings of the National Academy of Sciences of the United States of America 2007;104(8):2667–2672. [PubMed: 17307879]
28. Rong G, Wang H, Skewis LR, Reinhard B, x, rn M. Nano Letters 2008;8(10):3386–3393. [PubMed: 18788826]
29. Aaron J, Nitin N, Travis K, Kumar S, Collier T, Park SY, Jose-Yacaman M, Coghlan L, Follen M, Richards-Kortum R, Sokolov K. Journal of Biomedical Optics 2007;12(3):034007. [PubMed: 17614715]
30. Schlessinger J. Cell (Cambridge, Massachusetts) 2000;103(2):211–225.
31. Burke P, Schooler K, Wiley HS. Molecular Biology of the Cell 2001;12(6):1897–1910. [PubMed: 11408594]
32. Jaramillo ML, Leon Z, Grothe S, Paul-Roc B, Abulrob A, O'Connor McCourt M. Experimental Cell Research 2006;312(15):2778–2790. [PubMed: 16806168]
33. Sorkin A, von Zastrow M. Nat Rev Mol Cell Biol 2002;3(8):600–614. [PubMed: 12154371]
34. Frens G. Nature (London), Physical Science 1973;241(105):20–22.
35. Kumar S, Aaron J, Sokolov K. Nat. Protocols 2008;3(2):314–320.
36. Gooi HC, Hounsell EF, Lax I, Kris RM, Libermann TA, Schlessinger J, Sato JD, Kawamoto T, Mendelsohn J, Feizi T. Bioscience Reports 1985;5(1):83–94. [PubMed: 2580573]
37. Zhu J-X, Goldoni S, Bix G, Owens RT, McQuillan DJ, Reed CC, Iozzo RV. Journal of Biological Chemistry 2005;280(37):32468–32479. [PubMed: 15994311]
38. Wiley HS, Shvartsman S, Lauffenburger DA. Journal: Trends in Cell Biology 2003;13(1):43–50.
39. Miller K, Beardmore J, Kanety H, Schlessinger J, Hopkins CR. Journal of Cell Biology 1986;102(2): 500–509. [PubMed: 2868013]
40. Travis, K.; Aaron, J.; Harrison, N.; Sokolov, K. Phenomenology of optical scattering from plasmonic aggregates for application to biological imaging and clinical therapeutics, 2008. Tuan, V-D.; Joseph, RL., editors. SPIE; 2008. p. 68690H
41. Mackowski DW. J. Opt. Soc. Am 1994;11(11):2851–2861.
42. Mackowski DW. Proc. R. Soc. Lond 1991;433(1889):599–614.
43. Mackowski DW, Mishchenko MI. J. Opt. Soc. Am. A 1996;13(11):2266–2278.
44. Stout B, Auger J-C, Lafait J. Journal of Modern Optics 2000;49(13):2129–2152.
45. Aaron J, de la Rosa E, Travis K, Harrison N, Burt JL, José-Yacamán M, Sokolov K. Optics Express 2007;16(3):2153–2167. [PubMed: 18542296]
46. Lidke DS, Nagy P, Heintzmann R, Arndt-Jovin DJ, Post JN, Grecco HE, Jares-Erijman EA, Jovin TM. Nature Biotechnology 2004;22(2):198–203.

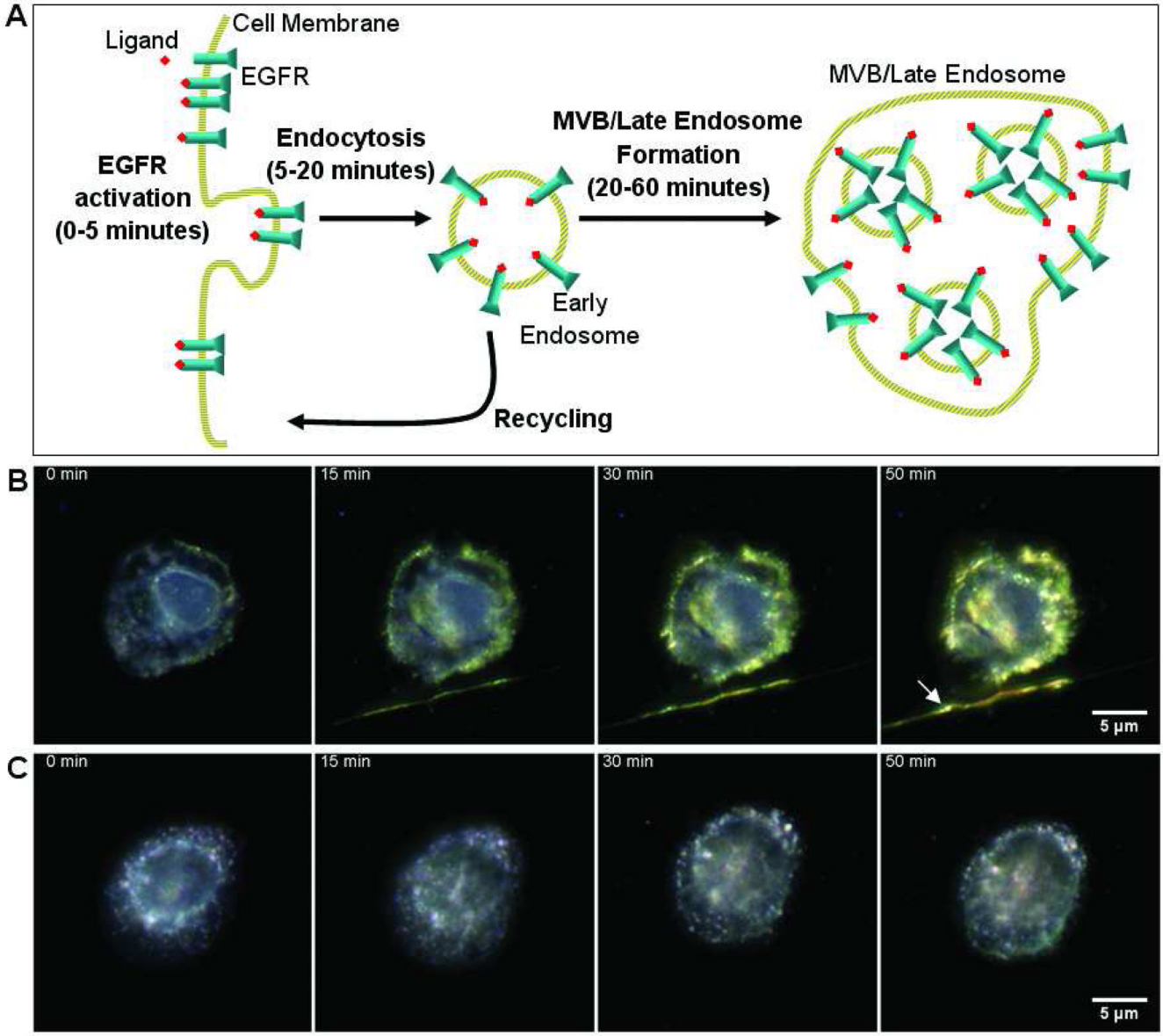

Figure 1.

Dynamic imaging of live cells. (A) A schematic of EGFR trafficking upon ligand binding. This process was monitored in real time in live cells labeled with anti-EGFR gold nanoparticles under the microscope: (B) live A431 cells and (C) live cells pre-treated with 10μM AG1478, which reduces endocytosis. From left to right, images show color and intensity changes in the gold nanoparticle optical signal at 0, 15, 30, and 50 minutes after initial exposure to nanoparticles. Darkfield images of untreated cells (B) display changes in color from blue to yellow-orange that are not present in treated cells (C). The arrow in (B, far right) indicates the presence of a filopodium emanating from an adjacent cell. Images were acquired using transmitted darkfield illumination and a long-working distance 63× 0.75 NA Objective.

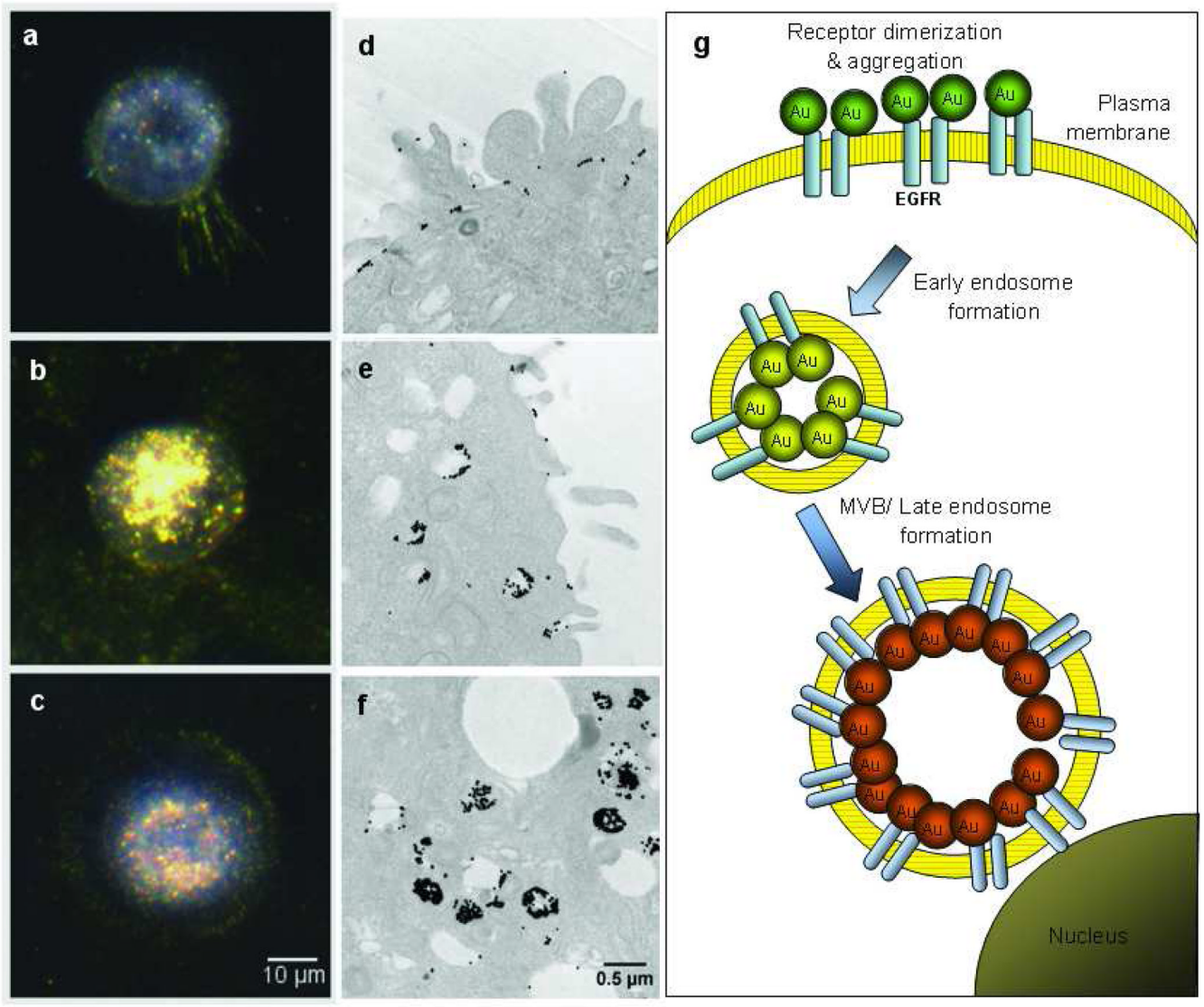

Figure 2.

Cells labeled at different temperatures. Darkfield images of A431 cells labeled with 25 nm anti-EGFR gold nanoparticle conjugates at 4°C (a), 25°C (b) and 37°C (c). Darkfield microscopy reveals light scattering from the samples. Controlling temperature arrests the normal EGFR regulatory processes at critical points, with receptors remaining on the cell membrane at 4°C, and endosomal internalization and multivesicular body sorting at 25°C and 37°C, respectively. Transmission electron microscopy (TEM) of identical samples (d - 4°C, e - 25°C, and f - 37°C) shows the nanometer-scale EGFR rearrangements which correspond to the optical images. In (g), a schematic illustrates the qualitative relationship between EGFR regulation state and optical signature of the associated gold nanoparticles.

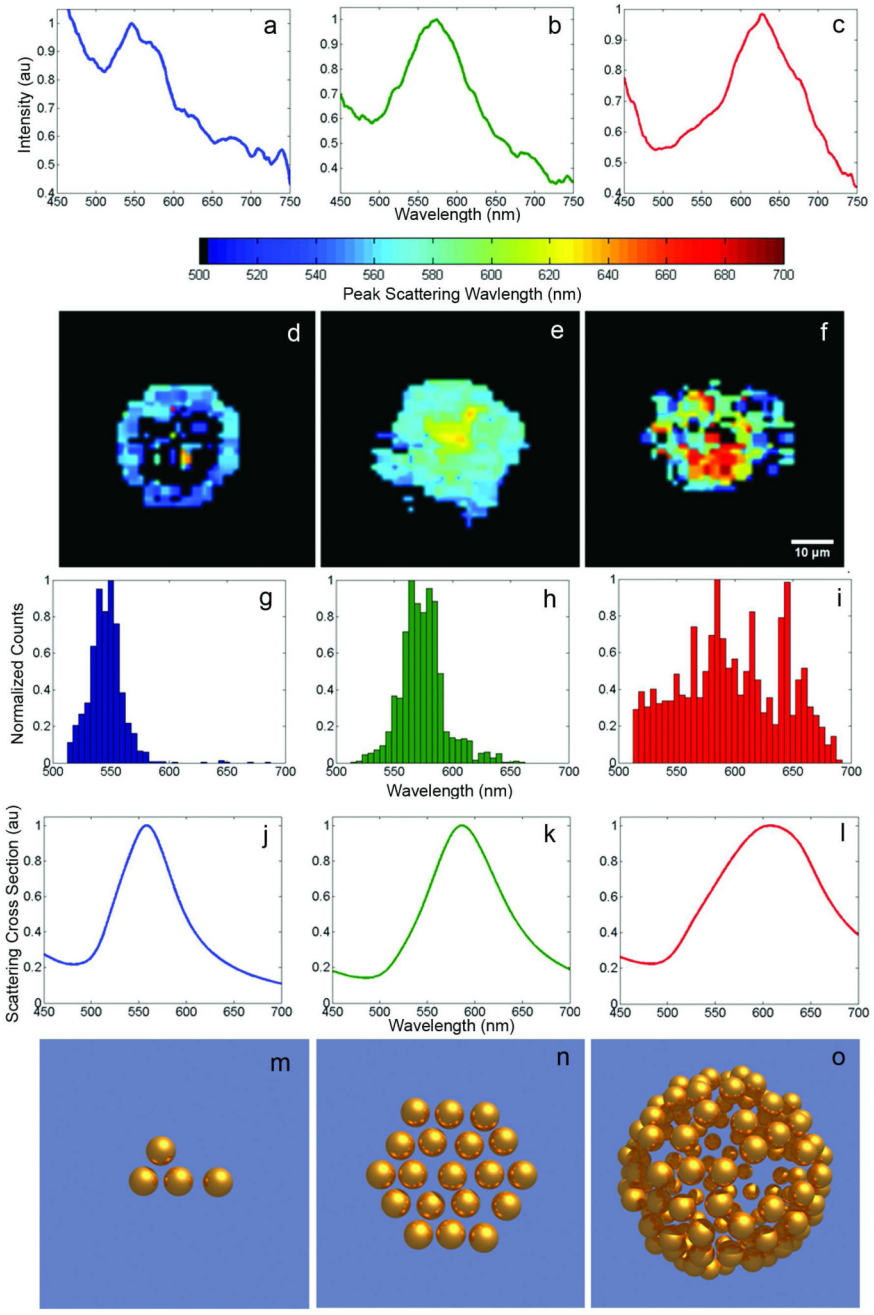

Figure 3.

Quantitative relationship between scattering from EGFR-bound gold nanoparticles and EGFR regulatory stages. Hyperspectral darkfield microscopy of cells labeled at 4°C (left column, a, d, g), 25°C (middle column, b, e, h) and 37°C (right column, c, f, i). The data was acquired using the microscope settings described in Figure 1. Representative single-pixel spectra from a cell image display scattering peaks at *ca.* 546 nm (a), 576 nm (b), and 601 nm (c). Cell images in (d–f) are color-coded according to the scattering peak position at each pixel in the field of view. Pixels that did not have an identifiable peak in a corresponding spectrum were not assigned a color. Distributions of the peak scattering wavelengths indicated in (d–f) are shown in (g–i). Electrodynamic simulations of scattering from nanoparticle aggregates are shown in

(j–l) for three typical structures: a 4-particle chain-like structure (j, m), a 19-particle disk-like structure (k, n), and a 130-particle volume-like structure (l, o). The total scattering cross section is plotted for each structure, alongside a rendering of the corresponding detailed particle arrangement (m–o). Distinct red-shifting and broadening of the scattering spectra is due to both the affect of the increased number of contributing particles and the effect of the transition from a 2D to a more 3-D volume-filling morphology.

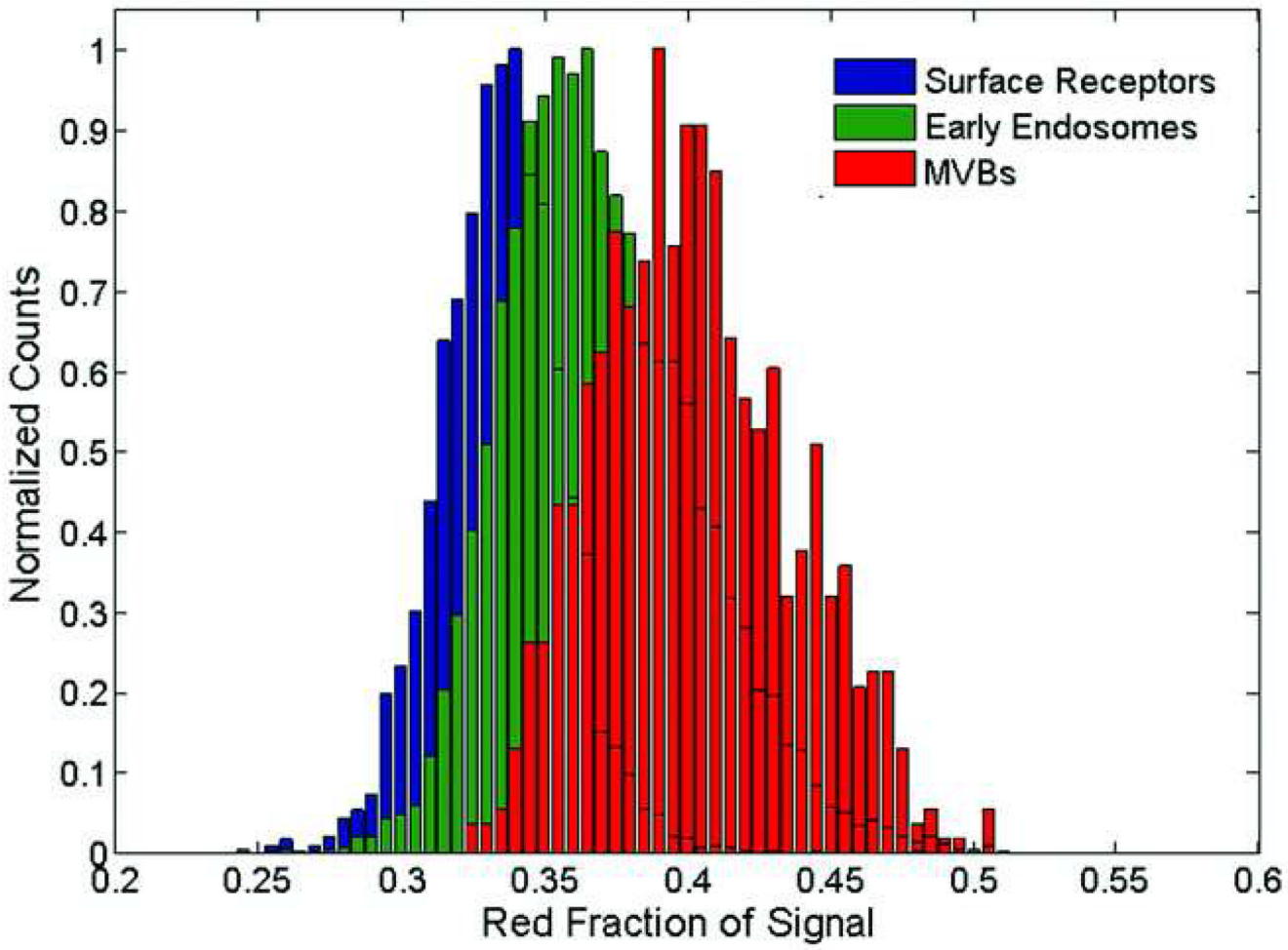

Figure 4.

Relative red channel intensity distributions for gold nanoparticle labeled EGFR molecules on the cell surface (blue), in early endosomes (green), and in late endosomes (red). For the CCD used, the red channel collects signal in the 600–700nm wavelength range. Increasing plasmon resonance coupling in each case results in an overall increase in red channel intensity. Live cell images from Figure 1 were analyzed on a pixel by pixel basis and compared with the three distributions shown via a statistical z-test.

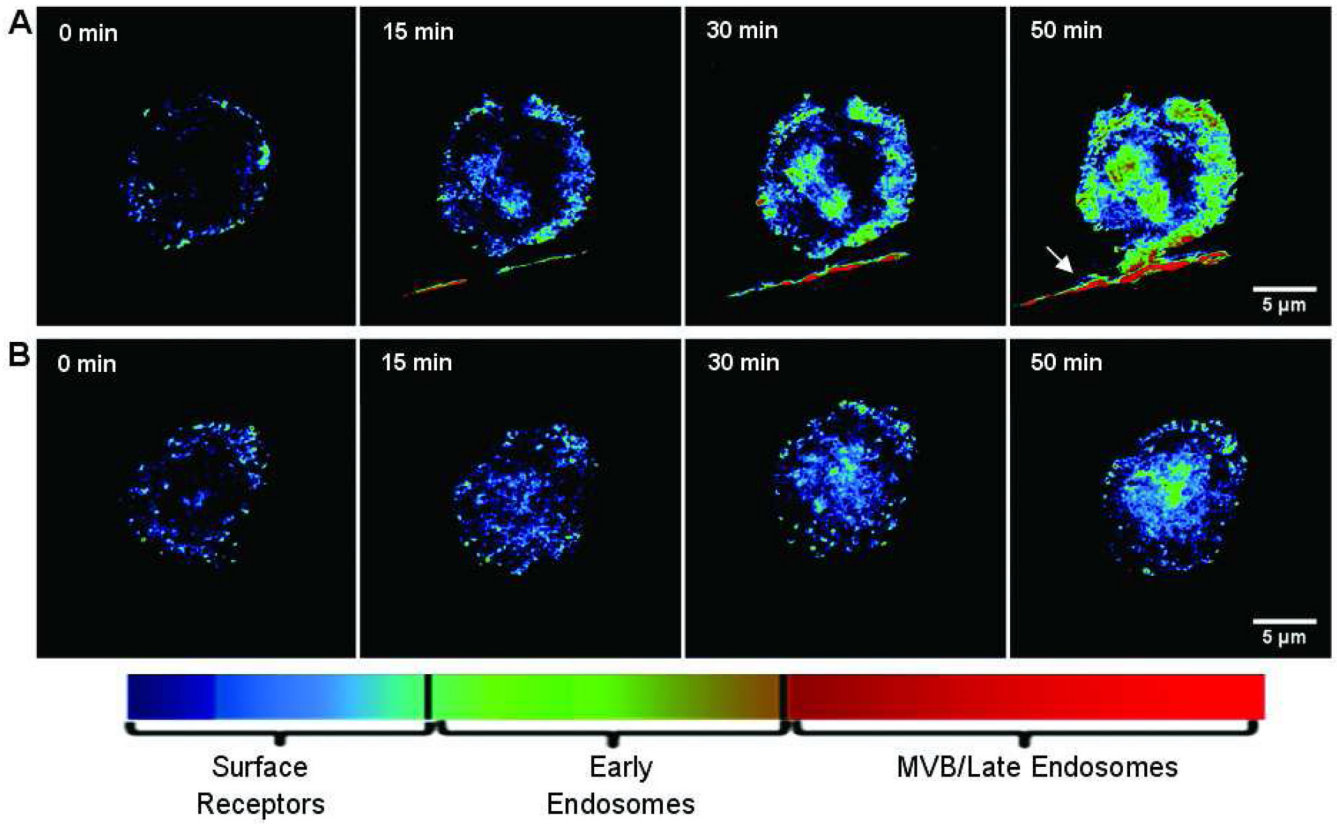

Figure 5.

Pseudo-color images of live cells representing distribution of EGFR regulatory stages. Statistical analysis of color time-lapse images shown in Figure 1 results in color-coded maps of EGFR distribution in untreated cells (A), and in cells after treatment with 10 μM AG1478 (B): a blue color indicated high probability that EGFR is located on the cytoplasmic membrane, green – in the early endosomes, and finally, red – in the late endosome/MVBs. Note that treatment with AG1478 markedly reduces endocytosis of EGFR. The arrow in (A, far right) indicates a filopodium emanating from an adjacent cell, which displays heavy EGFR trafficking along its axis.